

# Optical microscopy via spectral modifications of a nano-antenna

T. Kalkbrenner,<sup>1,\*</sup> U. Håkanson,<sup>1</sup> A. Schädle,<sup>2</sup> S. Burger,<sup>2</sup> C. Henkel,<sup>3</sup> and V. Sandoghdar<sup>1,†</sup>

<sup>1</sup>Laboratory of Physical Chemistry, Swiss Federal Institute of Technology (ETH), 8093 Zurich, Switzerland

<sup>2</sup>Zuse Institute Berlin, Takustrasse 7, 14195 Berlin, Germany.

<sup>3</sup>Institute of Physics, University of Potsdam, 14469 Potsdam, Germany.

The existing optical microscopes form an image by collecting photons emitted from an object. Here we report on the experimental realization of microscopy without the need for direct optical communication with the sample. To achieve this, we have scanned a single gold nanoparticle acting as a nano-antenna in the near field of a sample and have studied the modification of its *intrinsic* radiative properties by monitoring its plasmon spectrum.

PACS numbers: 07.79.Fc, 42.50.Lc, 42.30.-d, 78.67.Bf

Over the years, several clever techniques such as dark-field, phase contrast, fluorescence, differential interference contrast, confocal, and scanning near-field microscopies have provided powerful ways of performing optical imaging. In all these methods, as in any other visual process, one "sees" an object when photons originating from it reach the detector. The details of the imaging mechanism depend sensitively on the intensity, phase and polarization of light both in the illumination and collection channels. The thought of recording optical images *without* receiving photons from the object, therefore, seems to be a contradiction in terms. In this Letter we show that this is indeed possible if one monitors the intrinsic spectral properties of a nanoscopic antenna scanned close to the sample.

When an oscillating dipole is placed in confined geometries its radiative properties, such as eigenfrequency and linewidth, are modified [1, 2]. In an intuitive picture these modifications are due to the interaction of the oscillating dipole with its image dipoles whereby the boundary materials and their distances to the oscillator determine the strength and phase of this interaction. In an alternative point of view the radiative changes are due to the modification of the density of photon states available for emission. In the context of recent developments in nano-optics, theoretical investigations have extended these concepts to subwavelength geometries and have shown that the linewidth [3, 4, 5, 6, 7] and the transition frequency [5, 6] of a dipole also respond sensitively to the optical contrast of its nanoscopic environment. Hence, it has been proposed that the spectral modifications of a nano-antenna could serve as the signal for a novel mode of Scanning Near-field Optical Microscopy (SNOM) [4, 5, 7]. Here we report on the first realization of this idea, using a single gold nanoparticle as a subwavelength antenna.

It is well known that the collective excitation of free electrons in metallic particles can give rise to plasmon resonances, depending on the size, shape, and index of refraction of the particle as well as the optical constants of its surrounding [8]. For a spherical particle placed in a homogenous medium, the plasmon spectrum can be cal-

culated using Mie theory based on a multipole expansion. For gold particles of diameter 100 nm or smaller the optical response is by large due to the dipolar mode of the plasmon excitation. Thus, a gold nanoparticle can be considered as a dipolar antenna with a well-defined resonance frequency and linewidth. Having a large polarizability, single gold nanoparticles can be optically detected even down to a size of about 5 nm [9]. Furthermore, the large quantum yield of a gold nanoparticle [10] makes it a suitable candidate for studying the radiative properties of its environment. Finally, compared to the commonly used systems such as single dye molecules or semiconductor nanocrystals, metallic nanoparticles have the decisive advantage that they are indefinitely photostable.

In our laboratory we have developed a procedure for mounting a single gold nanoparticle to the end of an uncoated glass fiber tip [11]. We have also reported on the realization of apertureless SNOM by detecting the intensity of the light scattered from the gold nanoparticle at a fixed wavelength [11]. In the current experiment we use the same kind of probe (particle diameter of 100 nm), but we now record its plasmon spectrum at every scan pixel. Figure 1a shows the principal elements of the experiment. White light from a xenon lamp is brought to the experimental stage via a multimode fiber with a core diameter of 100  $\mu\text{m}$ , passed through a polarizer and weakly focused onto the tip end by using a lens system. The scattered light is collected by a microscope objective, di-

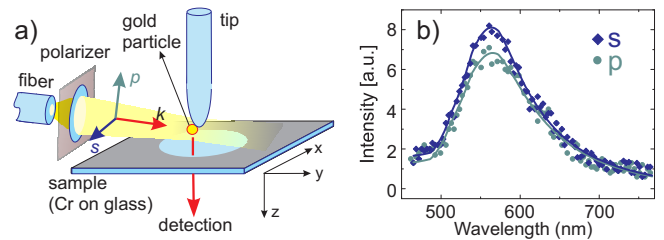


FIG. 1: a) Schematics of the experimental arrangement. b) Plasmon spectra of the gold nanoparticle attached to the glass fiber tip in the absence of the sample. The polarization of the incident light is indicated by s and p defined in a).

rected through a pinhole, coupled into a multimode fiber, and sent to a spectrometer equipped with a cooled CCD camera. Figure 1b displays scattering spectra of a gold nanoparticle at the end of the tip after it was picked up but away from the substrate. The diamonds and circles show the recorded spectra for  $s$  and  $p$  polarized incident light, respectively. The fact that the  $s$  and  $p$  spectra are nearly identical lets us conclude that the cross-section of the particle facing the incident beam is to a very good approximation circular [12].

A suitable sample for our studies should have a minimal topography, large optical contrast with sharp edges and be sufficiently transparent to allow detection in transmission. To fabricate such a sample, first we spin coated latex spheres of diameter  $2\ \mu\text{m}$  on a microscope cover slip at a very low coverage. Next we evaporated about  $8\ \text{nm}$  of chromium and removed the latex beads. The resulting sample consists of  $2\ \mu\text{m}$  round openings in a semi-transparent Cr film on a cover glass with very sharp edges that rise within less than  $10\ \text{nm}$  [11]. This sample was placed on a 3D piezoelectric scanner, mounted on an inverted microscope. A home-made SNOM stage was used to position the tip and to stabilize its distance from the sample to about  $5\text{-}10\ \text{nm}$  via shear-force feedback [13]. Figure 2a shows the shear-force topography image recorded when the sample was scanned under the gold nanoparticle probe, whereas the inset displays a cross section along cut (ii) (see Fig. 2c). The elevated annulus (height of about  $30\ \text{nm}$ ) in the middle of the glass region is produced by the collection of residual material at the junction between the latex particles and the substrate in the spin casting and lift-off processes.

During the shear-force scan shown in Fig. 2a the spectrometer camera was triggered at each of the  $1600$  pixels, and the plasmon spectrum of the gold particle was recorded. The symbols in Fig. 3a show spectra from pixels  $\alpha$  and  $\beta$  marked in Fig. 2a. Fig. 2b displays the total intensity integrated over the wavelength range  $450\text{-}750\ \text{nm}$  for each pixel. As expected, the signal is higher when the gold nanoparticle is on the glass part of the sample [11], but the intensity distribution is somewhat smeared out at the edges because we have not discriminated against unwanted far-field stray scattering. Efficient separation of the near-field signal from the stray background is also a central issue in conventional apertureless SNOM using extended tips [14, 15, 16, 17, 18].

Now we discuss the essential results of our work, namely the modifications of the particle's plasmon spectrum. Comparison of the spectra in Fig. 3a reveals a red shift and a broadening of  $\alpha$  with respect to  $\beta$ . While it is not possible to state a simple analytic formula for the spectrum of the nanoparticle in the near field of an inhomogeneous sample, we have found that we can fit our experimental data using a phenomenological model. In order to quantify the observed spectral modifications, we adapted the formalism of Wokaun, Gordon and Liao [19]

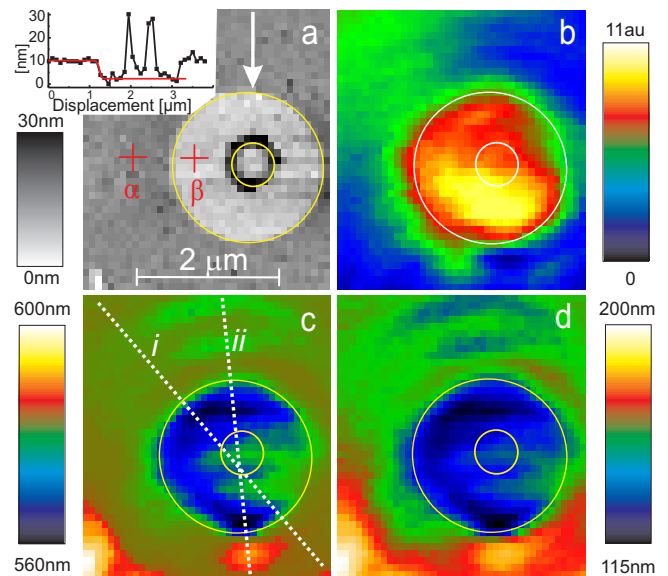


FIG. 2: a) Topography image of the sample ( $40 \times 40$  pixels), showing the round opening in a very thin chromium film. Inside this opening a small round protrusion is revealed (see text for details). The inset shows a cross section along cut (ii). The arrow indicates the direction of illumination. b) The transmitted intensity integrated under the spectrum recorded at each pixel. c) and d) The central wavelength and the FWHM of the plasmon resonance, respectively. The circles are traced as a guide to the eye.

based on the definition of an effective polarizability for a metallic nanoparticle. These authors showed that the total induced dipole moment  $P(\omega)$  of a nanoparticle with volume  $V \ll \lambda^3$  and dipolar polarizability  $\alpha(\omega)$  is given by

$$P(\omega) = \alpha(\omega) [E_0 + i\eta(2k^3/3)P(\omega)] \quad (1)$$

where  $E_0$  denotes the applied external electric field and  $k = 2\pi/\lambda$ . The first term in Eq. (1) considers the dipole moment that is induced directly by the incident field. The second term describes the so-called radiation damping effect where the field emitted by the particle interacts with its own dipole moment  $P(\omega)$ . In the original work of Wokaun and coworkers  $\eta$  was set to 1, but here we have introduced this real parameter in a phenomenological manner to represent the part of the particle's self field caused by reflections from the surroundings. We note that since we are dealing with near-field interactions, retardation effects could be neglected at this point. Rearrangement of Eq. (1) leads to an expression for the effective dipolar polarizability,

$$\alpha_{eff}(\omega) = \frac{P(\omega)}{E_0} = \frac{\alpha(\omega)}{1 - \eta[i2k^3\alpha(\omega)/3]}. \quad (2)$$

The solid curves in Fig. 1b represent theoretical fits to the particle plasmon resonance in the absence of a substrate; i.e.  $\eta$  was set to 1. Here the detected intensity

was taken to be proportional to the scattering cross section and therefore to  $k^4 |\alpha_{eff}(\omega)|^2$ , using the quasi-static polarizability  $\alpha(\omega)$  [8, 12]. Following the same procedure, but leaving  $\eta$  as a variable parameter, we then fitted the plasmon spectra of the gold particle in the immediate vicinity of the sample. The solid curves in Fig. 3a show examples of the fits obtained for spectra  $\alpha$  and  $\beta$ . The dashed lines display the linear functions that have been added to the radiated intensity of the particle to account for the background scattered light. The excellent signal-to-noise ratio and the robust fit to the experimental spectra allow us to determine even small changes in the peak positions and the full widths at half maxima (FWHM) of the spectra. The results for all scan pixels are displayed in Figs. 2c and d. The circular glass opening in the chromium film is clearly imaged in both cases. Figures 3b and c display cross sections of Figs. 2c and d along cut (*i*). As expected, the near-field coupling of the antenna to the lossy excitations in the chromium film causes a red shift and a broadening of its resonance when it is moved from the glass region to above the Cr-film [20]. These results embody the essence of this novel near-field imaging mechanism where the information about the local optical contrast of the sample is "encoded" in the spectrum of the nano-antenna and not in the field, phase or polarization of the received photons.

We now discuss some details of the images in Fig. 2. To facilitate this, we have overlaid circles as guides to the eye. These were first matched to the circular features of the topography image and then overlaid onto images 2c and d, allowing for a lateral offset due to a commonly observed displacement between the position of the gold nanoparticle and the lowest edge of the tip that traces the topography. We note that images 2c and d are much sharper than that in 2b where the overall scattered intensity is plotted. Furthermore, it is interesting that the central circular sedimentation does not appear in Figs. 2c and d, presumably because its refractive index is not very different from that of glass. There are, however, modulations of the resonance wavelength and linewidth in the illumination direction, both on the Cr-film and within the glass opening. We will discuss these below, but before doing so, we present numerical calculations that provide quantitative agreement with the magnitudes of the observed spectral shift and broadening.

Consideration of experimental parameters such as the finite size of the gold particle, its distance to the sample, the thickness of the Cr-film (less than a skin depth) and the interface between chromium and glass calls for rigorous numerical simulations. To do this, we have used the finite-element method to solve the time-harmonic Maxwell's equations in a two-dimensional setting for the magnetic field component  $H_x$  perpendicular to the computational plane. We took the tabulated dielectric functions for gold [21] and chromium [22] and implemented the Sommerfeld radiation condition with a special perfectly matched layer adapted to the structure of the ex-

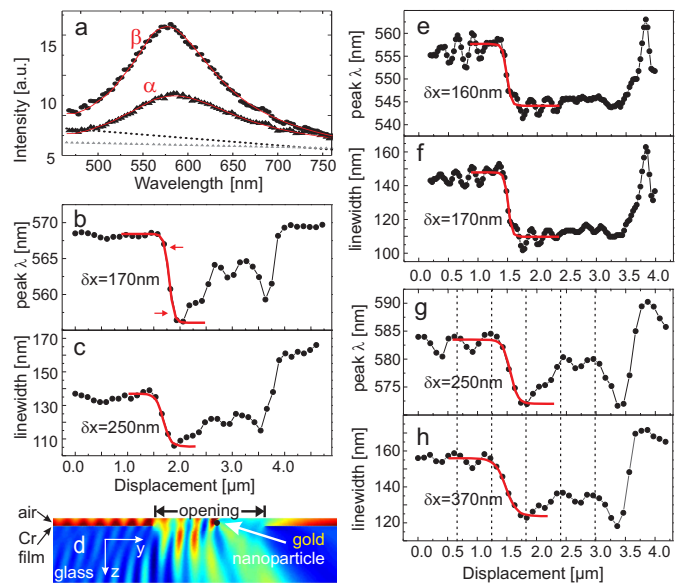


FIG. 3: a) Examples of the spectra recorded on the chromium and glass regions at positions  $\alpha$  and  $\beta$  in Fig. 2. Peak wavelengths and linewidths from cross sections *i* and *ii* in Fig. 2 are shown in (b, c) and (g, h), respectively. d) An example snapshot of the simulated distribution of intensity  $|H_x|^2$ . Due to lack of space, we only show the central part of the computation box. e) and f) Simulated peak wavelength and linewidth of the plasmon spectra for a 2D system. The red curves show fits by the edge function  $\tanh((y - y_0)/l)$  where  $y_0$  and  $l$  are free parameters. In each case the parameter  $\delta x$  represents the width from the 90% to 10% value of this function.

periment [23]. Figure 3c displays a snapshot of the intensity distribution  $|H_x|^2$  at  $\lambda = 570$  nm for a particular particle position. We determined the energy flux scattered into the detection numerical aperture from the angular spectrum representation of the field at the lower border of the simulation box, which was  $7.4 \mu m$  wide. By repeating the calculations for a large number of wavelengths, we obtained spectra that we fitted using the same procedure used for the experimental spectra. Figures 3e and f display the central wavelength and the FWHM of the calculated spectra as a function of particle position. For comparison, in Figs. 3g and h we also show the experimental data along the illumination direction corresponding to cut (*ii*) in Fig. 2. In both the theoretical and experimental curves we find about 30 nm broadening and 10 nm of red shift in the plasmon resonance as the particle is moved from the glass to the chromium section of the sample. The agreement between the experimental and theoretical findings is quantitative even though the calculations were only two-dimensional.

Next, we turn to the issue of modulations in Figs. 2c and d, which appear on both Cr and glass sections. The dashed lines in cross sections 3g and h indicate that these modulations repeat at a period of about 580 nm, which is of the order of the particle plasmon resonance wavelength  $\lambda_{res}$ . The key issue is that although we have minimized

the collected stray light by illumination at grazing incidence and by placing a pinhole in the detection path, the edges of the circular opening can scatter a non-negligible amount of light onto the detector. This background field interferes with the radiation of the particle at the detector (note that as shown in Fig. 3a, the background is much smaller than the particle radiation). As described in the supplementary material [30], scanning the sample results in an apparent modulation of the peak wavelength and linewidth of the plasmon spectrum at a period of about  $\lambda_{res}$ . Interestingly, Figs. 3e and f also display periodic modulations but this time at a period of about  $\lambda_{res}/2$ . Indeed, as indicated in Fig. 3d, there are strong standing waves that can be traced to the interference of the particle backscattering and the illumination fields around the sample. These fast modulations are, however, an artefact of 2D considerations which overestimate backscattering as compared to 3D geometries. Finally, we have checked that due to the large absorption of Cr, the coupling of the particle emission to surface plasmons [24] in the Cr film plays a negligible role in all these processes.

As a last point, we remark that the spatial resolution of our method depends on the size of the antenna. In our current experiment, however, the observed edge sharpness of 170-370 nm in Figs. 3 have been strongly influenced by the above-mentioned modulations, preventing us from determining the true resolution of the system. This source of artefact could be fully eliminated if imaging were performed via the measurement of the excited-state lifetime of a nanoscopic fluorescent emitter.

In conclusion, we have demonstrated that the intrinsic spectral properties of a nano-antenna can be used to probe the near-field optical contrast of a sample. The interesting aspect of this novel experiment is that there is neither a need to illuminate the sample, nor to receive light from it; instead one has to excite a subwavelength radiating dipole and measure the changes in its radiative characteristics. Although in the present work we have used photons to "read out" the spectrum of the antenna, one could imagine achieving this via electronic excitation of plasmon resonances [25] or by using electrical excitation of luminescent material [26, 27]. Changes of polariton or plasmon resonances in scanning probe microscopy have been also addressed in recent experiments where a tip interacts with an extended open geometry [28, 29]. Here we have realized an experiment where the modification of a well-defined *localized* plasmon resonance due to its near-field interaction with the sample has been put into evidence. Future experiments using very small gold nanoparticles [9] or fluorescent emitters promise to push the resolution of our method to the nanometer level.

We thank B. Buchler and S. Kühn for fruitful discussions. This work was supported by the Swiss National Foundation (SNF), ETH Zurich, Deutsche Forschungsgemeinschaft (DFG) priority program SPP 1113 and the DFG Research Center MATHEON.

- 
- \* Present address: FOM-Institute for Atomic and Molecular Physics, 1098 SJ Amsterdam, The Netherlands  
 † Electronic address: vahid.sandoghdar@ethz.ch
- [1] W. L. Barnes, *J. Mod. Optic* **45**, 661 (1998).
  - [2] P. R. Berman, *Cavity Quantum Electrodynamics* (Academic Press, 1994).
  - [3] L. Novotny, *Appl. Phys. Lett.* **69**, 3806 (1996).
  - [4] A. Rahmani, P. C. Chaumet, F. de Fornel, and C. Girard, *Phys. Rev. A* **56**, 3245 (1997).
  - [5] C. Henkel and V. Sandoghdar, *Opt. Commun.* **158**, 250 (1998).
  - [6] M. Quinten, *Appl. Phys. B* **67**, 101 (1998).
  - [7] G. Parent, D. Van Labeke, and D. Barchiesi, *J. Opt. Soc. Am. A* **16**, 896 (1999).
  - [8] U. Kreibig and M. Vollmer, *Optical Properties of Metal Clusters* (Springer Berlin, 1995).
  - [9] K. Lindfors, T. Kalkbrenner, P. Stoller, and V. Sandoghdar, *Phys. Rev. Lett.* **93**, 037401 (2004).
  - [10] B. C. Buchler, T. Kalkbrenner, C. Hettich, and V. Sandoghdar, submitted (2005).
  - [11] T. Kalkbrenner, M. Ramstein, J. Mlynek, and V. Sandoghdar, *J. Microsc.* **202**, 72 (2001).
  - [12] T. Kalkbrenner, U. Håkanson, and V. Sandoghdar, *Nano Lett.* **4**, 2309 (2004).
  - [13] J. Barenz, O. Hollricher, and O. Marti, *Rev. Sci. Instrum.* **67**, 1912 (1996).
  - [14] F. Zenhausern, Y. Martin, and H. K. Wickramasinghe, *Science* **269**, 1083 (1995).
  - [15] Y. Inouye and S. Kawata, *Opt. Lett.* **19**, 159 (1994).
  - [16] P. Gleyzes, A. C. Boccaro, and R. Bachelot, *Ultramicroscopy* **57**, 318 (1995).
  - [17] M. Labardi, S. Patanè, and M. Allegrini, *Appl. Phys. Lett.* **77**, 621 (2000).
  - [18] F. Keilmann and R. Hillenbrand, *Phil. Trans. R. Soc. London A* **362**, 787 (2004).
  - [19] A. Wokaun, J. P. Gordon, and P. F. Liao, *Phys. Rev. Lett.* **48**, 957 (1982).
  - [20] R. R. Chance, A. Prock, and R. Silbey, *Adv. Chem. Phys.* **31**, 1 (1978).
  - [21] P. B. Johnson and R. W. Christy, *Phys. Rev. B* **6**, 4370 (1972).
  - [22] P. B. Johnson and R. W. Christy, *Phys. Rev. B* **9**, 5056 (1974).
  - [23] L. Zschiedrich, R. Klose, A. Schädle, and F. Schmidt, to appear in *J. Comp. Appl. Math.* (2005).
  - [24] B. Hecht, H. Bielefeldt, L. Novotny, Y. Inouye, and D. W. Pohl, *Phys. Rev. Lett.* **77**, 1889 (1996).
  - [25] A. Degiron, H. Lezec, N. Yamamoto, and T. Ebbesen, *Opt. Comm.* **239**, 61 (2004).
  - [26] N. Kuck, K. Lieberman, and A. Lewis, *Appl. Phys. Lett.* **61**, 139 (1992).
  - [27] M. Baier, C. Constantin, E. Pelucchi, and E. Kapon, *Appl. Phys. Lett.* **84**, 1967 (2004).
  - [28] J. Aizpurua, G. Hoffmann, S. P. Apell, and R. Berndt, *Phys. Rev. Lett.* **89**, 156803 (2002).
  - [29] T. Taubner, F. Keilmann, and R. Hillenbrand, *Nano Lett.* **4**, 1669 (2004).
  - [30] See supplementary material for a detailed description of this effect.

Supplementary material for "Optical microscopy using the spectral modifications of a nano-antenna" by T. Kalkbrenner, U. Håkanson, A. Schädle, S. Burger, C. Henkel, and V. Sandoghdar

We treat the issue of modulations observed both in peak position and linewidth along the direction of illumination, both on the Cr and glass parts of the sample (see Figs. 2c, 2d, and 3g and 3h of the Letter). We believe that the modulation is caused by the interference between the particle radiation and the stray light scattered by the edge(s) of the chromium film. In our experiment the illumination and therefore the light scattered by the edges are white. The light scattered by the particle, on the other hand, follows its plasmon spectrum. Figure 4a below shows the schematic essence of the situation at hand, where we have replaced the sample by a localized white scatterer (this is justified because the pinhole in our detection path only selects light from a very small region of the sample). Let us consider the gold particle to be fixed. For simplicity, we can take its radiation spectrum to be a Lorentzian of width  $\gamma$ , centered at frequency  $\omega_0$  (see Fig. 4b). The electric field of the light scattered by the particle can be written,

$$E_{part}(\omega) = A_{part} \frac{\gamma/2}{\gamma/2 - i(\omega - \omega_0)}. \quad (3)$$

The electric field of the background light can be written as,

$$E_{bg}(\omega, z) = A_{bg} e^{i\omega z/c}, \quad (4)$$

where  $z$  is defined as the path difference between the particle emission and that of the background light (see Fig. 4a). Here we have taken the paths from the gold particle and the white scatterer to be about equal, which is a very good assumption for a far detector. Note that  $z \approx y$  for grazing incidence. The total intensity at the detector is thus given by

$$I_{tot}(\omega, z) = |E_{part}(\omega) + E_{bg}(\omega, z)|^2. \quad (5)$$

To approximate our experimental conditions, we take  $\gamma = 0.2\omega_0$  and consider the intensity of the background light to be about 10% of the maximum particle radiation. Now we let  $z$  vary (i.e. we scan the sample). Each wavelength component of the background field and the particle field interfere differently, leading to a slight modification of the line shape. Fig. 4c shows examples of the resulting spectrum for four distinct path differences. Fig. 4d shows the same information in grey scales over a displacement of about  $3\lambda_0$ . Note that although the resulting spectra are no longer truly Lorentzian, one can still attribute a line center and FWHM to them.

Figures 4e and f show the FWHMs and peak frequencies of these spectra, which turn out to oscillate by a small amount. The oscillations are not periodic, but for small displacements one can recognize a period of about  $\lambda_0 = \omega_0/2\pi c$ . This picture is in very good agreement with the observation of the small modulations in our experimental data.

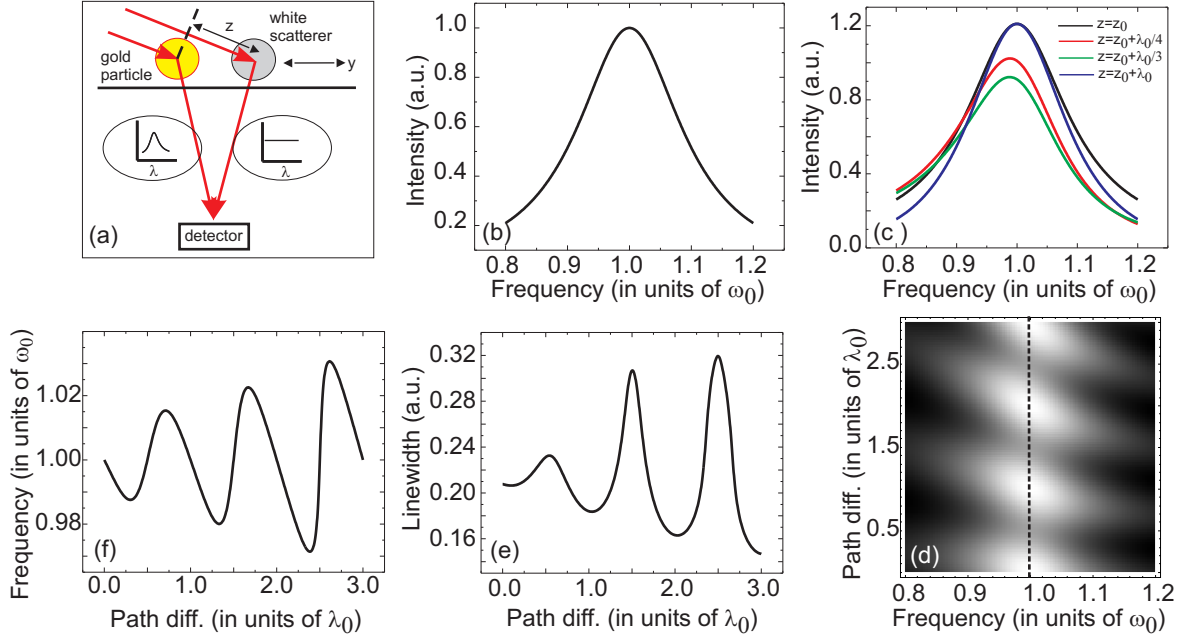


FIG. 4: (a) Schematics of the situation. (b) A broad Lorentzian spectrum. (c) Four examples of the resulting spectra.  $z_0$  denotes the zero path difference. (d) Contour plot of the total intensity as a function of the frequency and path difference. The linewidth (e) and peak position (f) along the cross section in (d).